



ISBN number for HWRS 2022 is 978-1-925627-64-0

# Modelling Fish-Friendly Culvert: an Academic Approach to a Practical Engineering Problem

Xinqian Leng<sup>1\*</sup> and Hubert Chanson<sup>2</sup>

<sup>1</sup> WSP Australia Pty Limited, Brisbane, Queensland, Australia

<sup>2</sup> School of Civil Engineering, University of Queensland, St. Lucia, Queensland, Australia

\* Corresponding author, email: [Sophia.leng@wsp.com](mailto:Sophia.leng@wsp.com)

## ABSTRACT

*Culverts are common hydraulic structures found under road embankments and low-level crossings, used to channel water through the road for drainage purposes. They have significant socio-economic values but can often act as barriers for upstream fish passage due to excessive flow velocity through the barrel. By conducting robust CFD modelling with detailed validations, new approach for fish-friendly culverts can be derived for smooth standard box culvert by optimising flood capacity for design flow, and upstream fish passage for a fraction of the design flow e.g.  $Q \leq 0.1Q_{des}$ , provided that the low velocity zone (LVZ) representing at least 15% of the flow area. Another approach is investigated by conducting detailed physical in a 12 m long 0.5 m wide box culvert barrel channel equipped with full-height sidewall baffles (design based upon rectangular sidewall baffles, proposed by DAF 2018), a fine characterisation of the hydrodynamics of the asymmetrical baffled culvert barrel is achieved. The results showed a very-significant impact of the full-height sidewall baffles on the turbulent flow conditions in the culvert barrel. The observations indicated in particular a substantial increase in flow turbulence and flow resistance, as well as an asymmetrical turbulent velocity field. The study demonstrated a massive reduction in discharge capacity of box culverts in presence of full-height sidewall baffles for a given design afflux, with an increasing impact with increasing discharge for all baffle configurations. The physical modelling data showed that the installation of full-height sidewall baffles proposed by DAF (2018) ( $h_b = 0.15$  m,  $L_b = 0.6$  m) would reduce by 77% of the capacity for a 0.9 m wide 12 m long single box culvert cell with baffles on both sides, including for an increased free-board to account for water surface instabilities. The two studies show how academic research methodologies can be adopted to investigate and provide solutions to practical engineering problems.*

## 1. INTRODUCTION

Culverts are common hydraulic structures found under road embankments and low-level crossings, used to channel water through the road for drainage purposes (Schall et al. 2012, QUDM 2016). Figure 1 shows typical culvert structures in Australia, including concrete box culverts, pipe culverts and minimum energy loss culverts.

Culverts have significant socio-economic values including transportation of local fish species and serving as hydrological control. As these structures are often designed with limited budget and prioritises capacity to pass flood during a critical event, they are known to have negative impacts on freshwater river system morphology and ecology, including the blockage of upstream fish passage

(Warren and Pardew 1998, Anderson et al. 2012, Chanson and Leng 2021). The manner in which waterway crossings block fish movement includes perched outlets and excessive vertical drop at the culvert exit, high velocity and insufficient water depth in the culvert barrel, debris accumulation at the culvert inlet, and standing waves in the outlet or inlet (Behlke et al. 1991, Olsen and Tullis 2013). All of which being closely linked to the targeted fish species. For small weak-swimming fish species, the upstream traversability of the culvert barrel is too often a major obstacle, particularly because of the fast water velocities.

Existing culvert guidelines to aid fish swimming upstream are typically based on three approaches:

- Putting restrictions on flow depth and velocity through the culvert (Fairfull and Whiteridge 2003)
- Placing in intrusive structures such as baffles or crossbars to create locally low velocity zones (DAF 2018)
- Implementing micro-roughness on internal faces of the culverts (DWA 2014)

There are a number of disadvantages associated with each approach. Simply putting restrictions on minimum water depth and maximum bulk velocity may yield expensive culvert structures. Figure 2 shows a retrofitted box culvert outlet with fish-friendly low-flow cell, costing around \$125,000. Implementing artificial roughness, such as baffles, crossbars and micro-roughness are expensive to install and maintain. Large baffles and crossbars can cause sediment deposition inside and downstream of the structure, significantly reducing flood capacity and sometimes posing as safety concern. Overall, constructions and rehabilitation of culverts for fish passage purposes in Australia are still limited by the restrictive nature and high cost of existing guidelines.



(a) Culvert outlet beneath Burdekin Falls Road QLD



(b) Pipe culvert outlet near Lower Tallebudgera Valley QLD



(c) Minimum Energy Loss (MEL) culvert inlet beneath the Gateway Freeway in Wynnum QLD

**Figure 1. Typical culvert structures in Australia (Photographs by Hubert CHANSON)**



**Figure 2. Retrofitted box culvert outlet with fish-friendly low-flow cell along Slacks Creek in Logan QLD, Australia; in 2018, the estimated cost is \$125,000. Photograph on 22 March 2021 about 14:30 (Photograph Hubert CHANSON)**

In this paper, two studies are reviewed to examine alternative design approaches to assist fish passage through culverts, especially small-bodied weak swimmers. The two studies used different research methodologies: one being a hybrid modelling combining CFD and experimental studies, with CFD being the main emphasis, the other one is a classic physical experiment with near-prototype-scale laboratory model. In the first study, a design approach without using baffles or any intrusive structures is proposed, based upon results collected from a series of numerical CFD simulations, with experimental data to support and validate the CFD results. This approach centres around the idea of providing adequate low velocity zones with a culvert barrel where small-bodied fish can traverse, at flood events that are a portion of the design flood events. In the second study, a design approach using various-sized sidewall baffles is proposed and examined, based upon laboratory experiments with relatively large-scale facilities, nearly 1:1. The study investigates the effectiveness of such baffles, and provide a quantitative estimate of capacity reduction caused by these baffles.

The two studies show how academic research methodologies can be adopted to investigate and provide solutions to practical engineering problems. These research methodologies are quick to apply with proper training, and are relatively low-cost with better accuracy compared to other methods used in current engineering practices.

## **2. METHODOLOGY**

### **2.1 Numerical modelling methodology**

#### **2.1.1 Navier-Stokes Equations and turbulence modelling**

CFD modelling of open channel flow through a culvert barrel was conducted with ANSYS<sup>TM</sup> Fluent version 18.0. A standard k- $\epsilon$  model was used to solve the flow turbulence (Rodi 1995). For smooth turbulent flow through simplistic geometries, the flow physics is mostly dominated by boundary shear on the bottom boundary. A simplistic turbulence model such as a k- $\epsilon$  model is sufficient to resolve the velocity field, with a relatively low computational cost. The k- $\epsilon$  model simplifies the Navier-Stokes

equations as:

$$\frac{\partial \rho}{\partial t} + \frac{\partial}{\partial x_j} (\rho u_j) = 0 \quad (1)$$

$$\frac{\partial \rho u_i}{\partial t} + \frac{\partial}{\partial x_j} (\rho u_i u_j) = -\frac{\partial p'}{\partial x_i} + \frac{\partial}{\partial x_j} \left[ \mu_{\text{eff}} \left( \frac{\partial u_j}{\partial x_j} + \frac{\partial u_j}{\partial x_i} \right) \right] + S_M \quad (2)$$

where  $S_M$  is the sum of body forces,  $\mu_{\text{eff}}$  is the effective viscosity representing flow turbulence, and  $p'$  is the modified pressure, the subscriptions  $i$  and  $j$  represent properties in the  $i$  and  $j$  directions. Based on the "eddy viscosity" concept proposed by Boussinesq (1897), the effective viscosity may be calculated as:

$$\mu_{\text{eff}} = \mu + \mu_t \quad (3)$$

where  $\mu$  and  $\mu_t$  are respectively the fluid viscosity and eddy (turbulent) viscosity.

The standard  $k$ - $\epsilon$  model used two transport equations to describe the turbulent viscosity. The two equations are for the turbulent kinetic energy  $k$  and dissipation  $\epsilon$  respectively (Launder and Spalding 1974):

$$\frac{\partial}{\partial t} (\rho k) + \frac{\partial}{\partial x_i} (\rho k u_i) = \frac{\partial}{\partial x_j} \left[ \left( \mu + \frac{\mu}{\sigma_k} \right) \frac{\partial k}{\partial x_j} \right] + G_k + G_b - \rho \epsilon - Y_M + S_K \quad (4)$$

$$\frac{\partial}{\partial t} (\rho \epsilon) + \frac{\partial}{\partial x_i} (\rho \epsilon u_i) = \frac{\partial}{\partial x_j} \left[ \left( \mu + \frac{\mu}{\sigma_\epsilon} \right) \frac{\partial \epsilon}{\partial x_j} \right] + C_{1\epsilon} \frac{\epsilon}{k} (G_k + C_{3\epsilon} G_b) - C_{2\epsilon} \rho \frac{\epsilon^2}{k} + S_\epsilon \quad (5)$$

where  $G_k$  represents the generation of turbulent kinetic energy due to the mean velocity gradient,  $G_b$  is the generation of turbulent kinetic energy due to buoyancy,  $Y_M$  represents the contribution of the fluctuating dilatation in compressible turbulence to the overall dissipation rate.  $C_{1\epsilon}$ ,  $C_{2\epsilon}$  and  $C_{3\epsilon}$  are constants,  $\sigma_k$  and  $\sigma_\epsilon$  are the turbulent Prandtl numbers for  $k$  and  $\epsilon$  respectively,  $S_k$  and  $S_\epsilon$  are user-defined source terms. The turbulent viscosity  $\mu_t$  is computed by combining  $k$  and  $\epsilon$  as:

$$\mu_t = \rho C_\mu \frac{k^2}{\epsilon} \quad (6)$$

By default, ANSYS Fluent used the following values for constants:  $C_{1\epsilon} = 1.44$ ,  $C_{2\epsilon} = 1.92$ ,  $C_\mu = 0.09$ ,  $\sigma_k = 1.0$ ,  $\sigma_\epsilon = 1.3$ .

The two-phase flow interface in the culvert barrel was tracked by a Volume of Fluid (VOF) method (Hirt and Nichols 1981). In VOF, a colour function  $C$  was introduced, defined as 0 in one phase and 1 in the other. Herein, the primary phase was selected to be air (the lighter medium) and secondary phase water. The function  $C$  is characterised by an advection equation:

$$\frac{\partial C}{\partial t} + \bar{u} \cdot \nabla C = 0 \quad (7)$$

Fluid properties such as density and viscosity are then calculated based on respective fractions of local colour function.

The near-wall areas of the flow were treated by a built-in standard wall function in ANSYS Fluent. The wall function was based on the work of Launder and Spalding (1974), and is used widely in industrial flows. The log-law was applied for near-wall regions to calculate the dimensionless velocity

$u^*$  by:

$$u^* = \frac{1}{\kappa} \ln(Ey^*) \quad (8)$$

where:

$$u^* \equiv \frac{u_p C_\mu^{1/4} k_p^{1/2}}{\tau_w / \rho} \quad (9)$$

and:

$$y^* \equiv \frac{\rho C_\mu^{1/4} k_p^{1/2} y_P}{\mu} \quad (10)$$

and  $\kappa$  is the von Karman constant ( $\kappa = 0.4187$ ),  $E$  is the empirical constant ( $E = 9.793$ ),  $U_p$  is the mean velocity of the fluid at the wall-adjacent cell centroid  $P$ ,  $k_p$  is the turbulence kinetic energy at the wall-adjacent cell centroid  $P$ ,  $y_p$  is the distance from the centroid of the wall-adjacent cell to the wall  $P$ , and  $\mu$  is the dynamic viscosity of the fluid. The law of the wall, i.e. log law, for mean velocity is only valid for  $30 < y^* < 300$  (Schlichting 1979, Chanson 2014). Herein, ANSYS Fluent employs the log law when  $y^* > 11.225$ . When the mesh yields  $y^* < 11.225$  at the wall-adjacent cells, ANSYS Fluent applies the laminar stress-strain relationship:

$$u^* = y^* \quad (11)$$

### 2.1.2 Numerical model configuration

The numerical domain representing a single-box culvert barrel is illustrated in Figure 3. Two barrel lengths were modelled, i.e.  $L_{\text{barrel}} = 8$  and  $12$  m. The width and height of the numerical domain were prescribed according to the internal width and height of the modelled culvert cells,  $B_{\text{cell}}$  and  $D_{\text{cell}}$  respectively. The definitions of each boundary are shown in Table 1. The inlet plane, marked in yellow and blue in Figure 3, was split into two velocity inlets, one for water (coded yellow) and one for air (coded blue). The outlet plane, coded green in Figure 3, was a single outlet for both phases, and set to be a pressure outlet. A free-surface level was required to set up the outlet for open channel flow, and this outlet depth  $d_{\text{out}}$  was prescribed according to the tailwater level for the modelled case. In general,  $d_{\text{out}} \approx d_{\text{tw}}$ , where  $d_{\text{tw}}$  was the tailwater depth in the floodplain downstream of the culvert barrel.

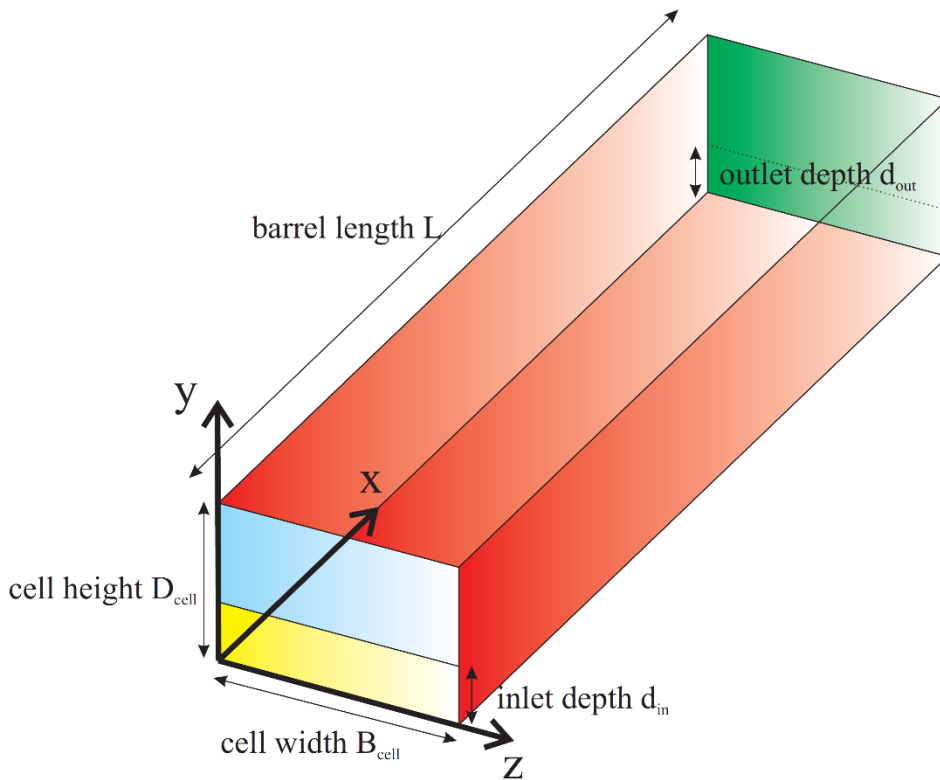


**Figure 3. Three-dimensional (3D) sketch of numerical domain with colour-coded boundaries; detailed boundary conditions listed in Table 1.**

**Table 1. Boundary conditions and colour-coding of boundaries as shown in Figure 3**

Colour	Boundary name	Boundary condition	Remarks
Blue	Air inlet	Velocity inlet	Inlet velocity $V_{in} = 0$ m/s
Yellow	Water inlet	Velocity inlet	Inlet velocity $V_{in}$ calculated from inlet discharge
Red	Walls	Wall	Roughness $k_s = 0-0.001$ m (i.e. smooth concrete). Uniform roughness
Green	Outlet (air & water)	Pressure outlet	Free-surface level at outlet $d_{out}$ set from tailwater level $d_{tw}$ ( $d_{out} = d_{tw}$ in general)

The numerical CFD modelling consisted of two stages: (1) transient flow simulation in a 3D culvert channel with coarse mesh; the coarse mesh consisted of uniform squares with 0.05-0.1 m grid size throughout the numerical domain; and (2) transient flow simulation in a 3D culvert channel with refined mesh; the mesh was refined into non-uniform gradually varied squares using a bias function:

$$\Delta = \sum_0^i \Delta_1 \times r^i \quad (12)$$

where  $\Delta$  is the size of the meshed edge,  $\Delta_1$  is the size of the first element calculated using a bias factor  $bf$ ,  $r$  is the growth rate,  $i = 1, 2, 3, \dots, n-1$  with  $n$  being the number of division in grid on the meshed edge. The relationship between growth factor  $r$ , bias factor  $bf$  and number of division  $n$  is:

$$bf = r^{n-1} \quad (13)$$

Biased mesh with refinement near the walls and sidewalls were essential to simulate realistic flow patterns near the boundaries. A bias factor of 20-30 was used typically for all cases, resulting in a growth factor  $r = 1.1-1.2$ . After refinement, the smallest grid size in the vertical  $y$  and transverse  $z$  directions was between 0.001 m to 0.005 m depending on the size of the culvert barrel. Due to the computational cost and limit in time, large culvert structures were meshed slightly coarser, compared to small culvert structures. The mesh in the stream-wise  $x$  direction was uniformly partitioned with a grid size of 0.05 m to 0.1 m for all cases.

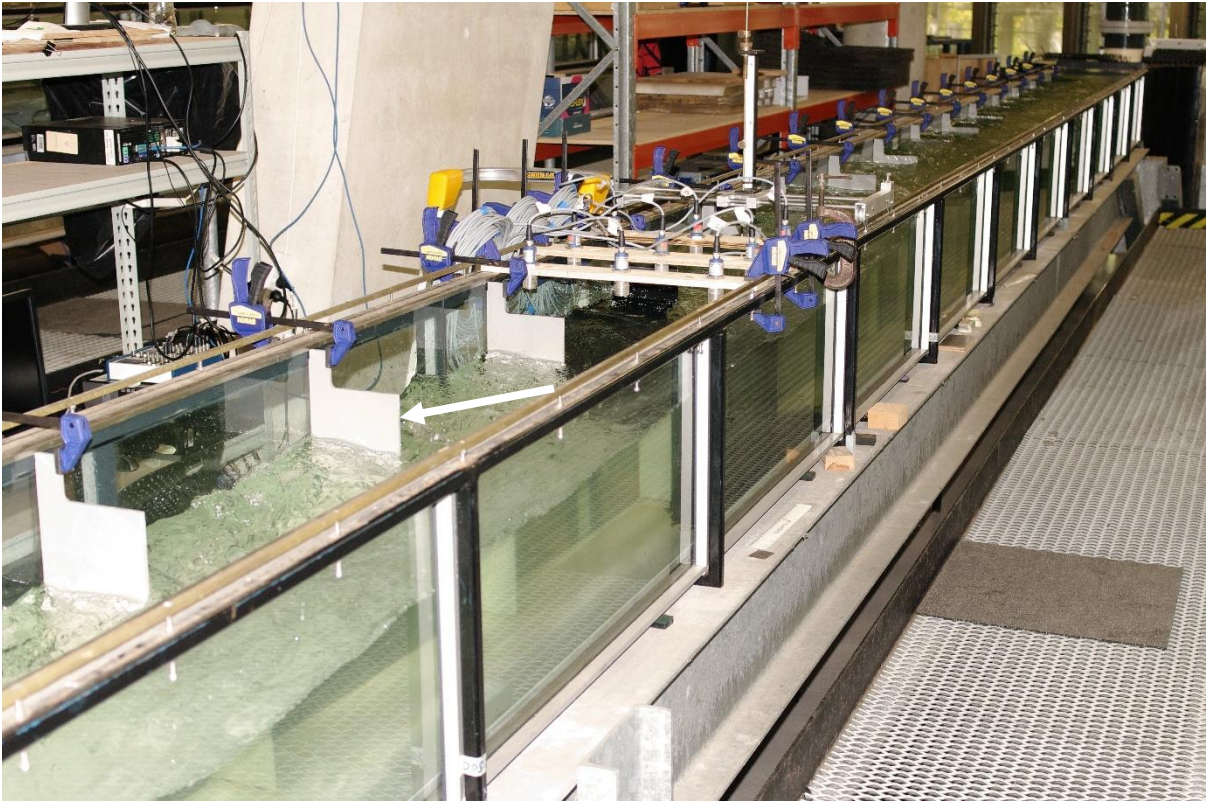
All models were solved using a  $k-\epsilon$  method for turbulence. The transient formulation was solved implicitly in first order, with a second order upwind scheme for momentum, first order upwind scheme for turbulent kinetic energy and turbulent dissipation rate. The convergence was ensured by reducing residuals of all parameters to  $10^{-4}$  or less. All simulations were run for a physical time span of over 90 s to ensure a steady equilibrium flow and the conservation of mass was achieved between inlet and outlet. The computation time for a complete run was approximately 12-24 hours on a HPC workstation.

## 2.2 Physical modelling methodology

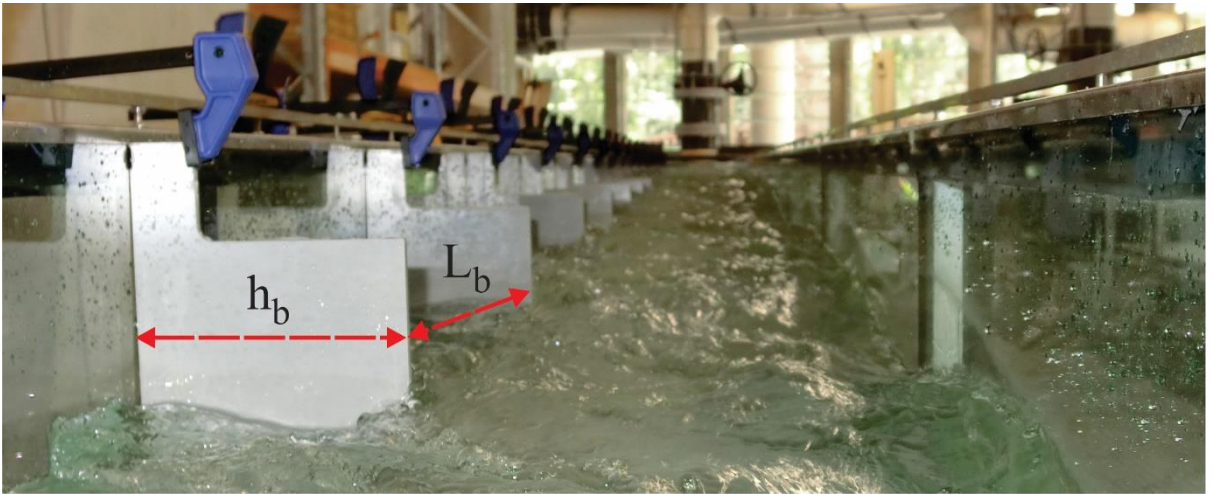
### 2.2.1 Experimental facilities

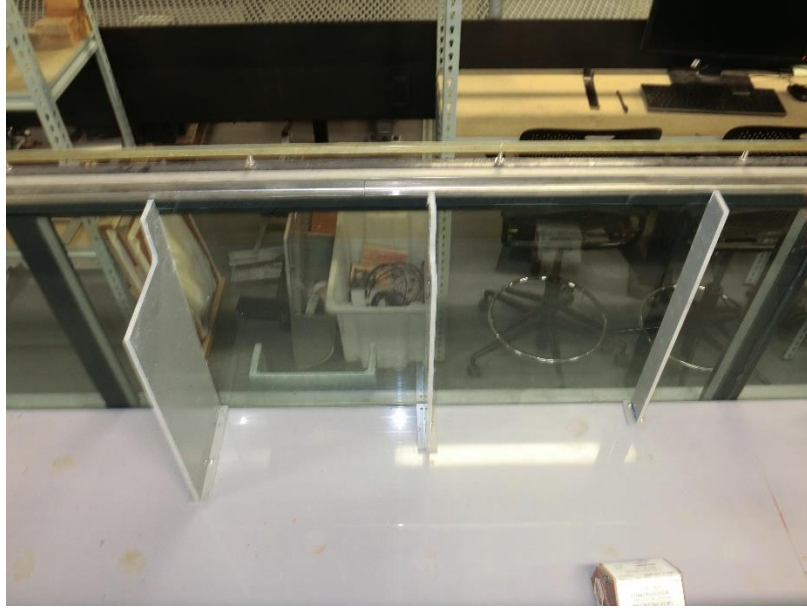
The investigation was conducted in a 15 m long and 0.5 m wide ( $B = 0.50$  m) tilting flume, previously used by Sanchez et al. (2018). The bed and sidewalls of the flume were made of PVC and glass respectively (Fig. 4). The bed of the channel was horizontal, i.e.  $S_o = \sin\theta = 0$  for all experiments. The flume was supplied water through a 2.0 m long 1.25 m wide intake structure, coming from a constant head tank, and equipped with baffles, flow straighteners and three-dimensional convergent leading to the 15 m long canal. The intake structure was design to deliver smooth inflow conditions into the channel. At the downstream end, the flume ended with a free overfall.

Figure 5 shows the definition sketch and photograph of the full-height sidewall baffles. Several boundary conditions were tested: (a) smooth channel without baffle; (b) small plain baffles ( $h_b = 0.042$  m); (c) medium baffles ( $h_b = 0.093$  m); and (d) large baffles ( $h_b = 0.167$  m), with  $h_b$  being the baffle size measure perpendicular to the right sidewall (Fig. 5). The smooth channel was used as reference. The plain baffles were full-height rectangular sidewall baffles, based upon DAF (2018). Figure 5 shows a side-by-side comparison of the various types of baffles. The baffles were made of 6 mm thick PVC sheets, cut with a water jet machine with tolerances of less than 0.2 mm. There were fixed to the floor and held at the top, as well as sealed to the sidewall



**Figure 4. Asymmetrical channel with full height sidewall baffles; looking upstream at the full height sidewall baffles. White arrow points to the baffles installed along the right sidewall.**





**Figure 5. Definition sketch (top) and full-height sidewall baffles in the dry channel [Bottom]; from right to left:  $h_b = 0.042$  m,  $0.083$  m,  $0.167$  m**

### 2.2.2 Instrumentation and calibration

The discharge was measured with a Venturi meter located on the water supply line, designed according to British standards (British Standard 1943), and with a percentage of error of the flow rate less than 2%. A pointer gauge was utilised to measure the free surface elevation with an accuracy of  $\pm 0.5$  mm.

A Prandtl-Pitot tube was used to measure the time-averaged velocity and pressure in the water (Leng and Chanson 2020). The Pitot tube was a Dwyer® 166 Series tube with a  $\text{Ø} = 1.19$  mm stainless steel tube. It featured a hemispherical total head tapping ( $\text{Ø} = 1.19$  mm) at the tip and four equally spaced static head tapplings ( $\text{Ø} = 0.51$  mm), located 25.4 mm behind the tip. The tip design met AMCA and ASHRAE specifications and the tube did not require calibration. The vertical translation of the Prandtl-Pitot tube was controlled by a fine adjustment travelling mechanism connected to a HAFCO® digital scale unit. The error on the vertical position of the probes was  $\Delta z < \pm 0.025$  mm. The accuracy on the longitudinal position was estimated as  $\Delta x < \pm 2$  mm. The accuracy on the transverse position of the probe was  $\pm 1$  mm.

The Prandtl-Pitot tube was further used to determine the shear stress at a boundary, i.e. the skin friction, when the tube is in contact with the wall (Preston 1954, Patel 1965, Macintosh 1990). The calibration of the Prandtl-Pitot tube showed that the boundary shear stress data followed closely an analytical solution of the Prandtl mixing length theory for turbulent boundary layer (Cabonice et al. 2017, 2019):

$$(\tau_o)_{\text{skin}} = \rho \times \kappa^2 \times \frac{V_b^2}{N^2} \quad (15)$$

where  $V_b$  is the velocity measured by the Prandtl-Pitot tube lying on the boundary,  $\kappa$  is the von Karman constant:  $\kappa = 0.4$ , and  $N = 7$  for a smooth turbulent boundary layer (Schlichting 1979, Liggett 1994).

The instantaneous velocities were measured with a Nortek™ Vectrino+ acoustic Doppler velocimeter (ADV), equipped with a sidelooking head (Hu et al. 2022). The ADV signal was sampled at 200 Hz

for 180 s at each location. All ADV signal data were postprocessed to remove erroneous data and spikes.

Particle tracking was conducted through the right sidewall using quasi-neutrally-buoyant spherical particles, sourced from Cospheric LLC (Li and Chanson 2020). The particle size was  $\text{\O}6.03$  mm and the relative density was  $s = 1.032$ .

The experiments were documented with dSLR cameras Pentax<sup>TM</sup> K-7 and K-3, a digital camera Casio<sup>TM</sup> Exilim EX-10, and digital camera Sony<sup>TM</sup> DSC-RX100M5A.

### 3. BOX CULVERT APPROACH: RESULTS AND DISCUSSION

A detailed validation of the present numerical model has been documented in Leng and Chanson (2019), based upon previous experimental findings (Cabonice et al. 2017), comparing free-surface profile and vertical profiles of the streamwise velocity. The validation concluded that the CFD data compared favourably to physical results for all transverse locations, with the locations next to the sidewalls being better modelled than the centre of the channel. The results showed an overall tendency of over-estimating longitudinal velocity magnitudes by the CFD numerical model, especially towards the centreline of the channel. The maximum longitudinal velocity was over-estimated by 10% using the CFD numerical model, compared to the experimental data for the flow  $Q = 0.056$  m<sup>3</sup>/s (Leng and Chanson 2019). Overall, the results showed the capacity of a CFD model to predict the three-dimensional flow field in a smooth culvert barrel, which could be used to design a fish-friendly culvert. The systematic validation against physical data is uppermost critical to ascertain the performances of a numerical model and can be sensitive to a range of inflow conditions, boundary parameters, and the grid mesh quality and size (Leng and Chanson 2019, Zhang and Chanson 2018).

Because of the large number of relevant design parameters (design discharge, tailwater level, maximum afflux, box cell configuration etc.) and the case specific nature of the culvert design (different targeted flood events for different regional councils), it is unrealistic to conduct CFD modelling for all possible design scenarios. Further, not all local governments and engineering companies have the capacity to conduct numerical CFD modelling. Hence, the calculation for percentage of flow area of low velocity zones must be generalised, with self-defined criteria for low velocity, independently of the hydrology requirement. That is, whether a targeted storm event is about 1:5 ARI or 1:1 ARI. Thus, the study examined the relationship between local velocity  $V_x$  and the associated flow area where the local velocity is less than that velocity. All data are compiled in a dimensionless form in Figure 7 for a wide range of flow conditions (Leng and Chanson 2019, Table 1).

Overall, all cases showed a similar trend, with quantitatively close results, albeit some scatter. The solid black curve represents the best-fit correlation of all datasets, whereas the two dashed lines illustrate the upper and lower bounds of the scatter. At an area fraction of 15%, the maximum difference between the two bounds of the data scatter was approximately 10%. The quantitative differences between data sets seemed to show little relation to the aspect ratio  $B/d$  of breadth to water depth.

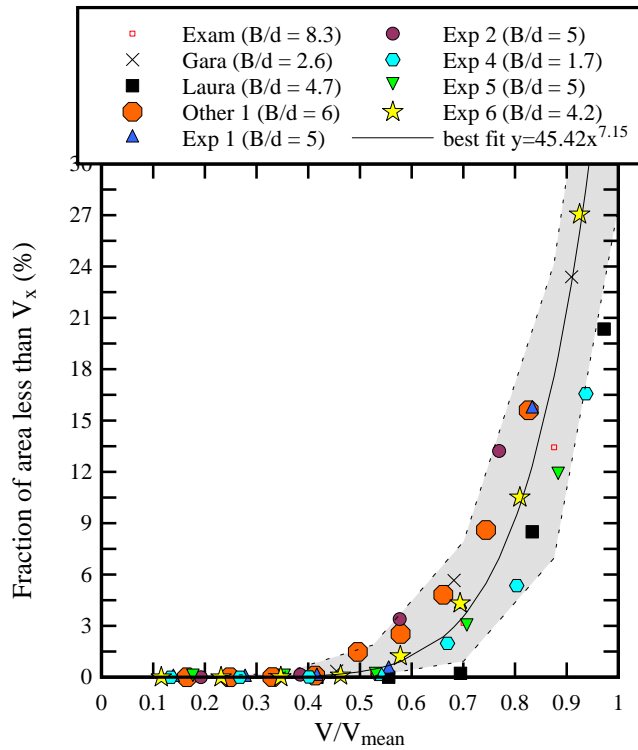


**Figure 7. Dimensionless area fraction of flow less than a relative longitudinal velocity  $V/V_{\text{mean}}$ , where  $V_{\text{mean}}$  is the bulk velocity i.e. cross-sectional mean velocity in the barrel; all cases compiled**

A comparison between physical and numerical CFD data is presented Figure 8. The data are compared to an analytical solution for a two dimensional turbulent flow, assuming a  $1/N$ -th velocity distribution power law:

$$A = 100^{1-N} \times \left( \frac{N}{N+1} \right)^N \times \left( \frac{V_x}{V_{\text{mean}}} \right)^N \quad (14)$$

with  $A$  the percentage of flow area,  $V_{\text{mean}}$  the bulk velocity,  $(V_x/V_{\text{mean}})$  in percentage. Equation 14 is plotted for  $N = 4.5$  in Figure 8. The present CFD results showed a close agreement with past CFD data, albeit limited to only a few points. The experimental data showed overall a larger area fractions for the same relative velocity compared to CFD data. The lower bound of experimental data scatter agreed closely with the upper bound of CFD data scatter.

It is worth to note several advantages of using such a dimensionless plot (Fig. 8). First the plot is independent of hydrological implication, which could vary upon requirement of different councils and sites. Second the results are independent of the barrel culvert cell size and downstream tailwater conditions.

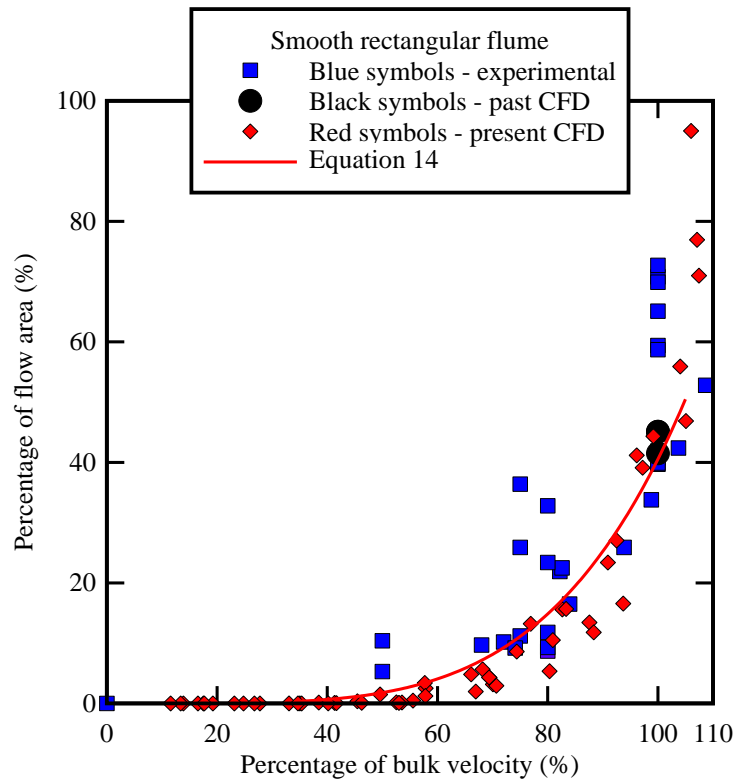


**Figure 8. Dimensionless area fraction of flow less than a relative longitudinal velocity  $V/V_{\text{mean}}$ , where  $V_{\text{mean}}$  is the bulk velocity i.e. cross-sectional mean velocity in the barrel; all cases compared to past CFD (Naot and Rodi 1982), experimental studies (Cabonce et al. 2017, Xie 1998, Macintosh 1990, Nezu and Rodi 1985, Nikuradse 1926), and Equation (14) assuming  $N = 4.5$**

#### 4. SIDEWALL BAFFLE APPROACH: RESULTS AND DISCUSSION

##### 4.1 Visual Observation

Visual observations were conducted using high-definition (HD) photographic camera (3000×4000 px) and video camera (1920×1080 px, 30 frames per second). Typical free-surface patterns are presented (Fig. 9). The intrusion of the full-height sidewall baffles roughened the flow, causing significantly more turbulence, forming visible turbulent structures from the flow surface and underneath the flow. Stagnation was observed as the right side of the flow was brought to rest by a baffle, resulting in a significant regional increase in upstream flow depth and a series of ripples leading up to it (Fig. 9a). The presence of baffles raised the water depth in the whole the channel. Downstream of the baffle, a wake zone was observed, highlighted by some swirling, small amount of aeration and low velocity flow behind the baffles (Fig. 9b and c). Some shock waves can be observed on the free-surface across the experimental channel (Fig. 9a, black arrows). Overall, the free-surface flow was very rough with strong coherent structures in presence of baffles.

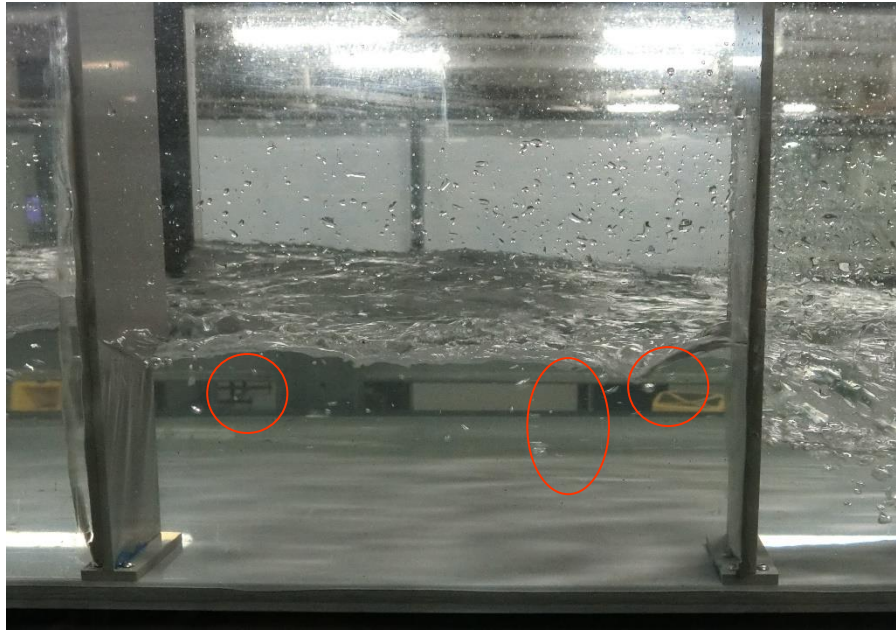
For the same baffle size, as the discharge increased, the flow became visibly more turbulent and the free-surface seemed rougher. When the longitudinal spacing between baffles increased, a more turbulent wake zone was created, highlighted by shaper separation around the edge of the baffle, larger decrease in water level before and behind the baffle, and sometimes more aeration in the wake. As the baffle size increased, the roughness of the flow increased, and the rise in water level was more significant throughout the channel, as one would expect.



(a) Free-surface flow pattern in an open channel with medium side wall baffles  $h_b = 0.083$  m, distance between baffles  $L_b = 0.333$  m, flow rate  $Q = 0.056$  m<sup>3</sup>/s



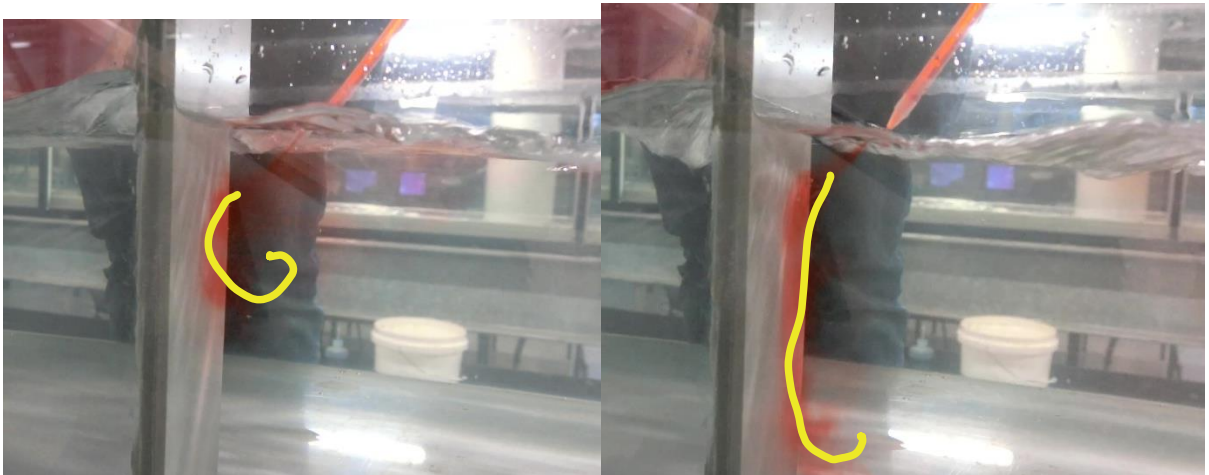
(b) Swirling flow structures observed in between two baffles ( $h_b = 0.083$  m,  $L_b = 0.333$  m,  $Q = 0.037$  m<sup>3</sup>/s)



(c) Aerations observed in between two baffles ( $h_b = 0.083$  m,  $L_b = 0.333$  m,  $Q = 0.056$  m<sup>3</sup>/s); the photograph shows the two most downstream baffles

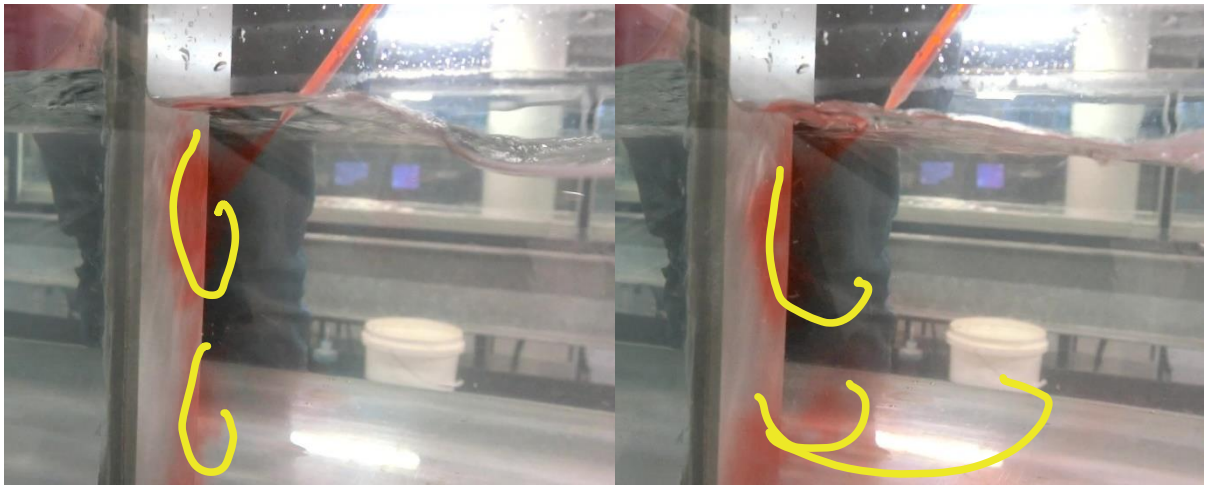
**Figure 9. Free-surface flow pattern in an open channel with medium side wall baffles  $h_b = 0.083$  m, distance between baffles  $L_b = 0.333$  m, flow rate  $Q = 0.056$  m<sup>3</sup>/s**

Further visualisations of flow patterns were conducted by injecting coloured dye or neutrally buoyant particles into the cavity flow. A marked low velocity zone was found behind baffles along the right side wall. Both dye and particles stayed and circulated for a period of time before disappearing. The visual observations also indicated the existence of shear zone occurring between the fast main flow region and low velocity region in the wake of baffles. Figure 10 illustrates typical flow structures visualised using dye injection behind a medium baffle, showing a main flow direction from left to right. The trajectories of the dye plume is highlighted by the yellow curves in Fig. 10.



(a) Flow pattern 1

(b) Flow pattern 2



(c) Flow pattern 3

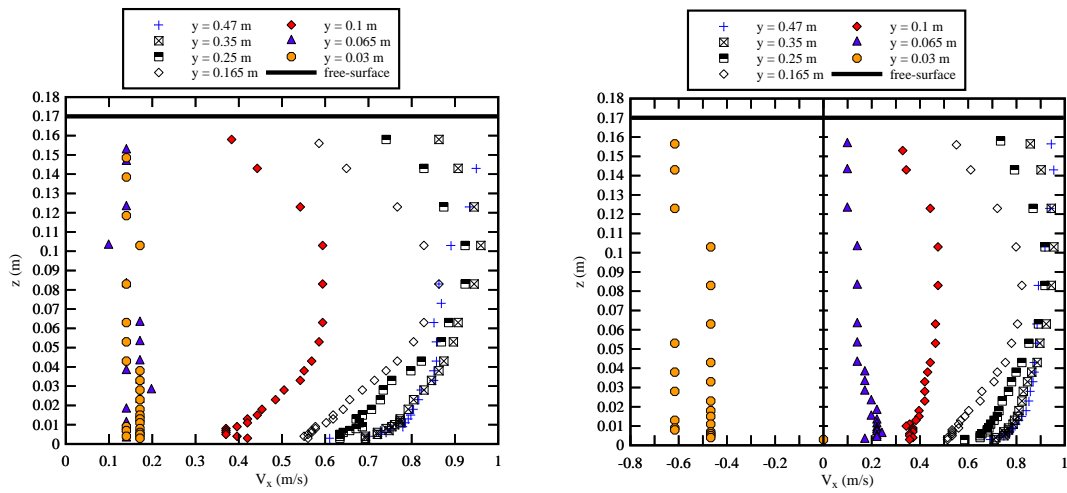
(d) Flow pattern 4

**Figure 10. Turbulence structures behind a baffle visualised using dye injection; flow direction from left to right;  $h_b = 0.083$  m,  $L_b = 0.333$  m,  $Q = 0.056$  m<sup>3</sup>/s**

#### 4.2 Streamwise Velocity Distributions with Sidewall Baffles

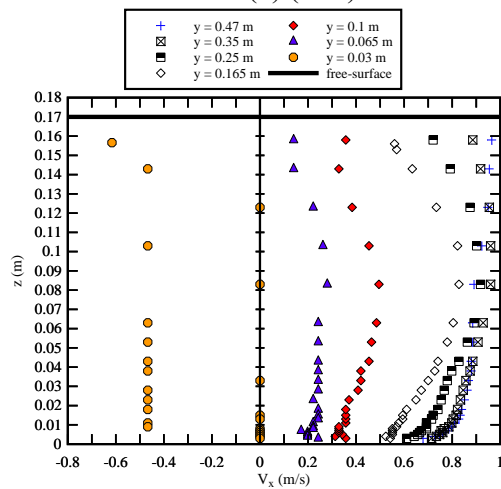
Velocity measurements were conducted, at three longitudinal locations:  $(x-x_b)/x_b = 0.05, 0.5$  and  $0.75$ . Herein,  $x_b$  referred to the longitudinal location of the reference baffle:  $x_b = 8.20$  m, where  $x$  was measured from the upstream end of the test flume. For each location  $(x-x_b)/L_b$ , the measurements were undertaken at several transverse distances to the sidewalls, from very close to the sidewalls ( $y = 0.0016$  m and  $0.4984$  m) to the channel centreline ( $y = 0.25$  m), where  $y$  is the distance to the right-side-wall. A full vertical profile of longitudinal velocity was recorded at each of the transverse location, to gain a comprehensive picture of the velocity distribution across the flow cross-section. A detailed summary of the flow and boundary conditions is presented elsewhere (Leng and Chanson 2020, Hu et al. 2022).

Figure 11 shows typical vertical distributions of streamwise velocity at different transverse distance from the sidewalls, for the three relevant distances from the baffles  $(x-x_b)/L_b = 0.05, 0.5$  and  $0.75$ . The thick black horizontal lines in all figures represented water free-surface measured at  $x = 8$  m. Altogether, the data showed a significant effect of the baffles in decelerating the flow, evidenced by decreasing velocity at all elevations with transverse distance closer to the baffle (right-side-wall). Some negative velocity was observed close to the baffled sidewall. Initially observed with the Prandtl-Pitot tube, the findings were confirmed with acoustic Doppler velocimetry (ADV).



(a)  $(x-x_b)/L_b = 0.05$

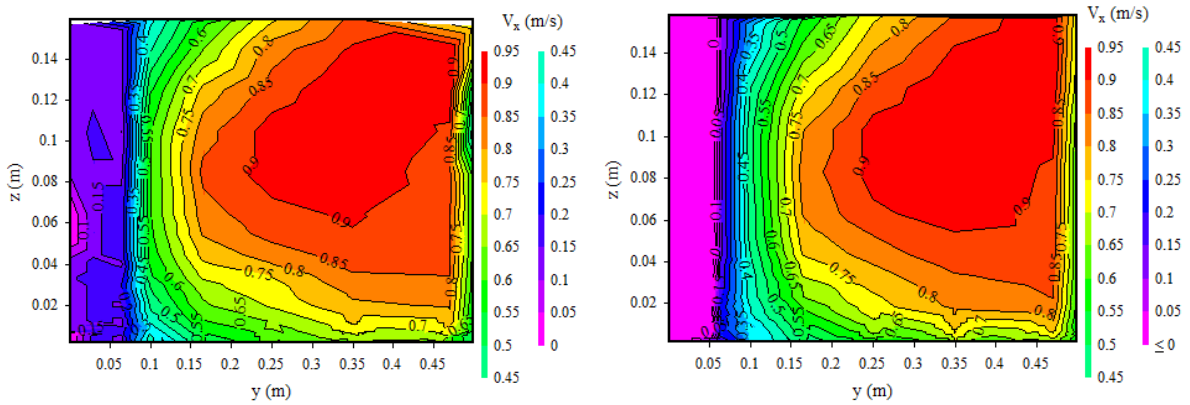
(b)  $(x-x_b)/L_b = 0.50$



(c)  $(x-x_b)/L_b = 0.75$

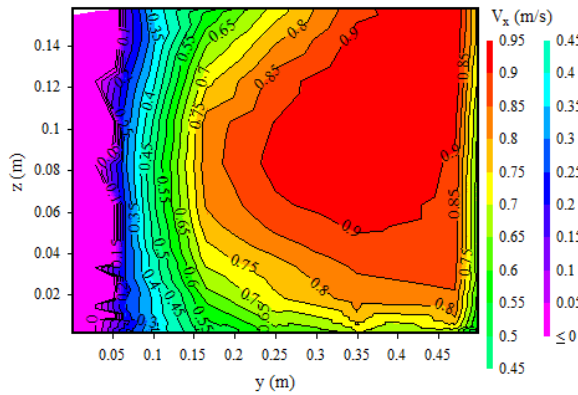
**Figure 11 - Vertical profile of streamwise velocity at distance  $(x-x_b)/L_b = 0.05, 0.50, 0.75$  behind a medium baffle; flow conditions:  $Q = 0.054 \text{ m}^3/\text{s}$ ,  $S_o = 0$ ,  $L_b = 0.33 \text{ m}$ , Prandtl-Pitot tube data**

Complete velocity contours for the three measured cross-sections are shown in Figure 13. The baffles were installed along the right sidewall, corresponding to the low velocity regions at  $y = 0-0.1 \text{ m}$  (Fig. 13). Overall, all data showed an asymmetrical distribution of the streamwise velocity as a result of the presence of baffles. The high velocity flow regions were shifted towards the left sidewall ( $y = 0.3-0.45 \text{ m}$ ), whereas a relatively low velocity zone was observed from the right sidewall to almost the centreline of the channel ( $y = 0-0.25 \text{ m}$ ). Immediately behind the baffles ( $y = 0-0.083 \text{ m}$ ), the velocity was very small, less than 32% of the cross-sectional mean velocity, sometimes negative. The low velocity zone behind baffles had a good connectivity between two adjacent baffles, as all measured cross-sections showed similar areas and magnitudes of low velocity.



(a)  $(x-x_b)/L_b = 0.05$

(b)  $(x-x_b)/L_b = 0.50$



(c)  $(x-x_b)/L_b = 0.75$

**Figure 13. Streamwise velocity contours of the flow cross-sections at distance  $(x-x_b)/x_b = 0.05, 0.50, 0.75$  behind a medium baffle; flow conditions:  $Q = 0.054 \text{ m}^3/\text{s}$ ,  $S_o = 0$ , water depth  $d = 0.17 \text{ m}$  measured at  $x = 8\text{m}$ , Prandtl-Pitot tube data**

### 4.3 Application and reduction in discharge capacity

Recent experimental studies by Li and Chanson (2020) and Hu et al. (2022) extended knowledge on sidewall baffles in culverts. Li and Chanson (2020) studied the hydrodynamic instabilities of open-channel flow past sequential lateral cavities in a relatively large facility. By using high-frequency free-surface sampling, the existence of fluctuations at a quasi-constant frequency less than that of gravity standing waves was confirmed. The trajectories of neutrally-buoyant particles were recorded within a cavity. The study also found that a 40% free-board need to be considered to account for the free-surface wave instabilities. Hu et al. (2022) conducted high-resolution measurements of the instantaneous flow velocity and found the existence of some low-frequency seiche phenomenon. A well-established triple decomposition technique was applied by Hu et al. (2020) to the time series of free-surface and velocity time-series. The low-pass components confirmed a unique flow structure, consisting of a high-velocity zone in the main channel and a low-velocity flow reversal within the lateral cavities. The band-pass components corresponded to the low frequency flow oscillations, highlighting the complicated transverse interactions between the lateral cavity and the main channel. The high-pass velocity components were related to the 'true' turbulence characteristics. The current study provides some further insights into the sustainable design of culverts to assist with upstream fish migration in man-made and natural fast waterways.

To sum up, considering a single cell box culvert with a 12 m long barrel ( $B = 2 \text{ m}$ ,  $D = 0.9 \text{ m}$ ),

comparative design calculations were completed for a smooth barrel and a barrel equipped with full-height sidewall baffles ( $h_b = 0.15$  m,  $L_b = 0.6$  m) on both sides (DAF 2018). In the former (smooth barrel), a free-board of 20%, i.e. clearance between the free-surface and obvert, at the design flow rate was considered. In the latter (sidewall baffled barrel), a 40% free-board was included to account for the free-surface wave instabilities. For inlet control, and with a 20% clearance between the water surface and obvert in the barrel, the discharge capacity of the smooth single-cell culvert barrel is  $3.825$  m<sup>3</sup>/s (Leng and Chanson 2020).

In presence of full-height sidewall baffles on both sides, and a 40% clearance between obvert and water surface, the discharge capacity of the baffled culvert is  $0.88$  m<sup>3</sup>/s for the same total head loss of  $0.384$  m. This corresponds to a reduction of the discharge capacity by 77%!

During the culvert operation, sediment and debris trapping by the baffles further may substantially restrain the discharge capacity of the structure, and in turn adverse negatively upstream fish passage. Thus, a broad maintenance plan has to be implemented to ensure that both the culvert barrel's low-velocity-zone and its longitudinal connectivity, as well as the culvert discharge capacity, are not adversely affected by sedimentation and debris trapping (Chanson and Leng 2021).

## 5. CONCLUSION

By conducting robust CFD modelling with detailed validations, a new hydraulic engineering guideline is derived based upon a number of basic design considerations (Chanson and Leng 2021):

- (a) smooth standard box culvert design, without appurtenance;
- (b) design optimisation for flood capacity for  $Q = Q_{des}$ , and for upstream fish passage for  $Q < Q_1$  e.g.  $Q_1 = 0.1 \times Q_{des}$ ; and
- (c) provision of low velocity zone (LVZ) representing at least 15% of the flow area and where  $0 < V_x < U_{fish}$  for upstream fish passage (i.e.  $Q < Q_1$ ), where  $U_{fish}$  is a characteristic fish speed, e.g. set by a regulatory agency or based upon biological observations and swimming test data.

The new approach relies upon a solid understanding of turbulence in box culvert barrel at less-than-design discharges, and an accurate physically-based knowledge of the entire velocity field in the culvert barrel, specifically the longitudinal velocity map, to accurately characterise the low velocity zone (LVZ) next to the barrel walls and corners. Although the focus of the present guidelines is on the upstream passage of small-body-mass fish, typical of Australian native fish species, the approach and methodology are relevant to most standard box culvert structures and can be applied to a much wider range of fish species including juveniles. The fundamental design considerations lead to a two stage hydraulic engineering design. First the minimum number of culvert barrel cells (or the smallest internal barrel dimensions for a single cell standard box culvert) is calculated to achieve inlet control at design flow conditions, based upon current standards for optimum flood capacity design at the culvert site. Second, considerations for upstream fish passage are embedded into the design method, using biological considerations. The revised fish-friendly culvert design may include a larger number of barrel cells than the original design. In such a case, the reduction in upstream flooding might contribute to some savings which could partially offset the increased cost caused by the larger culvert barrel dimensions. The method is more general than previous attempts, yet simple and cost effective enough to be widely endorsed by the various stakeholders. By bridging the gap between engineering and biology, this novel approach may contribute to the restoration of catchment connectivity.

By conducting detailed physical in a 12 m long 0.5 m wide box culvert barrel channel equipped with full-height sidewall baffles (design based upon rectangular sidewall baffles, proposed by DAF 2018), a fine characterisation of the hydrodynamics of the asymmetrical baffled culvert barrel is achieved. The results showed a very-significant impact of the full-height sidewall baffles on the turbulent flow conditions in the culvert barrel. The observations indicated in particular a substantial increase in flow turbulence and flow resistance, as well as an asymmetrical turbulent velocity field. The study

demonstrated without a doubt a massive reduction in discharge capacity of box culverts in presence of full-height sidewall baffles for a given design afflux, with an increasing impact with increasing discharge for all baffle configurations. The physical modelling data showed that the installation of full-height sidewall baffles proposed by DAF (2018) ( $h_b = 0.15$  m,  $L_b = 0.6$  m) would reduce substantially the design discharge capacity of the culvert barrel. For example by 77% of the capacity for a 0.9 m wide 12 m long single box culvert cell with baffles on both sides, including for an increased free-board to account for water surface instabilities. In practice, the increased wave height necessitates a larger clearance. In many cases when the discharge capacity cannot be compromised or the total costs including maintenance become exorbitant, alternative designs should be considered to assist upstream fish passage, e.g. small corner baffles (Cabonce et al. 2019), asymmetrical roughness (Wang et al. 2018).

### ACKNOWLEDGEMENT

The authors acknowledge the contributions made by Professor Colin J. APELT, Dr Matthew GORDOS, Marcus RICHES, Dr Hang WANG. The authors thank Jason VAN DER GEVEL and Stewart MATTHEWS (The University of Queensland) for their technical assistance

### REFERENCE

- Anderson, G.B., Freeman, M.C., Freeman, B.J., Straight, C.A., Hagler, M.M., and Peterson, J.T. (2012). "Dealing With Uncertainty When Assessing Fish Passage Through Culvert Road Crossings." *Environmental Management*, Vol. 50, pp. 462-477.
- Behlke, C.E., Kane, D.L., McLeen, R.F., and Travis, M.T. (1991). "Fundamentals of Culvert Design for Passage of Weak-Swimming Fish." Report FHW A-AK-RD-90-10, Department of Transportation and Public Facilities, State of Alaska, Fairbanks, USA, 178 pages.
- Boussinesq, J. (1897), "Essai sur la théorie des eaux courantes." *Mémoires présentés par divers savants à l'Académie des Sciences*, Vol. 23, No. 1, pp. 1-680 (in French).
- British Standard (1943). "Flow Measurement." British Standard Code BS 1042:1943, British Standard Institution, London.
- Cabonce, J., Fernando, R., Wang, H., and Chanson, H. (2017). "Using Triangular Baffles to Facilitate Upstream Fish Passage in Box Culverts: Physical Modelling." Hydraulic Model Report No. CH107/17, School of Civil Engineering, The University of Queensland, Brisbane, Australia, 130 pages (ISBN 978-1-74272-186-6).
- Cabonce, J., Wang, H., and Chanson, H. (2018). "Ventilated Corner Baffles to Assist Upstream Passage of Small-Bodied Fish in Box Culverts." *Journal of Irrigation and Drainage Engineering*, ASCE, Vol. 144, No. 8, Paper 0418020, 8 pages (DOI: 10.1061/(ASCE)IR.1943-4774.0001329).
- Cabonce, J., Fernando, R., Wang, H., and Chanson, H. (2019). "Using Small Triangular Baffles to Facilitate Upstream Fish Passage in Standard Box Culverts" *Environmental Fluid Mechanics*, Vol. 19, 23 pages (DOI: 10.1007/s10652-018-9604-x).
- Chanson, H. (2014). "*Applied Hydrodynamics: An Introduction*." CRC Press, Taylor & Francis Group, Leiden, The Netherlands, 448 pages & 21 video movies (ISBN 978-1-138-00093-3).
- Chanson, H., and Leng, X. (2021). "*Fish Swimming in Turbulent Waters. Hydraulics Guidelines to assist Upstream Fish Passage in Box Culverts*." CRC Press, Taylor and Francis Group, Leiden, The Netherlands, 202 pages and 19 video movies (DOI: 10.1201/9781003029694) (ISBN 978-0-367-46573-5 [Hardback]; 978-1-003-02969-4 [e-book]).
- DAF (2018). "Accepted development requirements for operational work that is constructing or raising waterway barrier works." Fisheries Queensland, Department of Agriculture and Fisheries, Australia, 77 pages.

- DWA (2014). "Fischaufstiegsanlagen und fischpassierbare Bauwerke – Gestaltung, Bemessung, Qualitätssicherung." Merkblatt DWA-M 509, Deutsche Vereinigung für Wasserwirtschaft, Abwasser und Abfall e. V., Hennef, Germany, 334 pages (ISBN 978-3-942964-91-3).
- Fairfull, S., and Witheridge, G. (2003). "Why do fish need to cross the road? Fish passage requirements for waterway crossings." NSW Fisheries, Cronulla NSW, Australia, 14 pages.
- Henderson, F.M. (1966). "*Open Channel Flow*." MacMillan Company, New York, USA.
- Hirt, C., and Nichols, B. (1981). "Volume of Fluid (VOF) method for the dynamics of free boundaries." *Journal of Computational Physics*, Vol. 39, No. 1, pp. 201-225.
- Hu, J., LI, Y., and Chanson, H. (2022). "Near-full-scale physical modelling and open-channel flow velocity in a fish-friendly culvert with full-height sidewall baffles." *Proc. 9th International Symposium on Hydraulic Structures ISHS2022*, Roorkee, India 24-27 October, 10 pages.
- Lauder, B.E., and Spalding, D. B. (1974). "The numerical computation of turbulent flows", *Computer Methods in Applied Mechanics and Engineering*, Vol, 3, No. 2, pp. 269-289 (DOI 10.1016/0045-7825(74)90029-2).
- Leng, X., and Chanson, H. (2019). "Hybrid Modelling of Low Velocity Zones in Box Culverts to Assist Upstream Fish Passage." *Environmental Fluid Mechanics*, Vol. 20, No. 2, pp. 415-432 (DOI: 10.1007/s10652-019-09700-1)
- Leng, X., and Chanson, H. (2020). "How Full-Height Sidewall Baffles affect Box Culvert Capacity: Balancing Fish Passage and Discharge Requirements." *Australasian Journal of Water Resources*, Vol. 24, No. 2, pp. 248-256 (DOI: 10.1080/13241583.2020.1824367).
- Li, Y., and Chanson, H. (2020). "Hydrodynamic Instabilities in Open-Channel Flow past Lateral Cavities." *Proceedings of 22nd Australasian Fluid Mechanics Conference AFMC2020*, Brisbane, Australia, 7-10 December, Published by The University of Queensland, Editors H. Chanson and R. Brown, Paper 26, 4 pages (DOI: 10.14264/4bf0316).
- Liggett, J.A. (1994). "*Fluid Mechanics*." McGraw-Hill, New York, USA.
- Macintosh, J.C. (1990). "Hydraulic Characteristics in Channels of Complex Cross-Section." Ph.D. thesis, University of Queensland, Department of Civil Engineering, Australia, November, 487 pages (DOI: 10.14264/uql.2015.218).
- Naot, D. and Rodi, W. (1982). "Numerical simulations of secondary currents in channel flow." *Journal of Hydraulic Division, ASCE*, Vol. 108, No. HY8, pp. 948–968.
- Nezu, I. and Rodi, W. (1985). "Experimental study on secondary currents in open channel flow." *Proceedings of the 21st IAHR Congress*, IAHR, Melbourne, pp. 115-119.
- Nikuradse, J. (1926). "Turbulente Stromung im Innem des rechteckigen offenen Kanals." *Forschungsarbeiten*, Heft 281, pp. 36-44 (in German).
- Olsen, A. and Tullis, B. (2013). "Laboratory Study of Fish Passage and Discharge Capacity in Slip-Lined, Baffled Culverts." *Journal of Hydraulic Engineering, ASCE*, Vol. 139, No. 4, pp. 424–432
- Preston, J.H. (1954). "The Determination of Turbulent Skin Friction by Means of Pitot Tubes." *Journal of Royal Aeronautical Society, London*, Vol. 58, Feb., p. 109-121.
- QUDM (2016). "Queensland Urban Drainage Manual." Institute of Public Works Engineering Australasia, Queensland Division, Brisbane, Australia, Fourth edition, 391 pages.
- Rodi, W. (1995). "Impact of Reynolds-Average Modelling in Hydraulics." *Proceedings Mathematical and Physical Sciences*, Vol. 451, No. 1941, pp. 141-164.
- Sanchez, P.X., Leng, X., and Chanson, H. (2018). "Fluid Dynamics and Secondary Currents in an

Asymmetrical Rectangular Canal with Sidewall Streamwise Rib." Hydraulic Model Report No. CH113/18, School of Civil Engineering, The University of Queensland, Brisbane, Australia, 158 pages (ISBN 978-1-74272-223-8)

Schall, J.D., Thompson, P.L., Zerges, S.M., Kilgore, R.T., and Morris, J.L. (2012). "Hydraulic Design of Highway Culverts." Hydraulic Design Series No. 5, Federal Highway Administration, Publication No. FHWA-HIF-12-0263rd edition, 326 pages.

Schlichting, H. (1979). "*Boundary Layer Theory*." McGraw-Hill, New York, USA, 7th edition.

Wang, H., Uys, W., and Chanson, H. (2018). "Alternative Mitigation Measures for Fish Passage in Standard Box Culverts: Physical Modelling." *Journal of Hydro-environment Research*, IAHR, Vol. 19, pp. 214-223 (DOI: 10.1016/j.jher.2017.03.001).

Warren, M.L., Jr., and Pardew, M.G. (1998). "Road crossings as barriers to small-stream fish movement." *Transactions of the American Fisheries Society*, Vol. 127, pp. 637-644.

Xie, Q. (1998). "Turbulent Flows in Non-Uniform Open Channels: Experimental Measurements and Numerical Modelling." Ph.D. thesis, School of Civil Engineering, The University of Queensland, Brisbane, Australia, 358 pages.

Zhang, G., and Chanson, H. (2018). "Three-Dimensional Numerical Simulations of Smooth, Asymmetrically Roughened, and Baffled Culverts for Upstream Passage of Small-bodied Fish." *River Research and Applications*, Vol. 34, No. 8, pp. 957-964 (DOI: 10.1002/rra.3346).

## BIOGRAPHY

Dr Sophia Leng researches in physical and numerical (CFD) modelling of unsteady turbulent flows, e.g. breaking waves, bores and positive surges, field investigations of tidal bores, and hydraulic design of fish-friendly culverts. Graduated in 2018 with a PhD in Civil Engineering (University of Queensland), she has authored and co-authored over 60 peer-reviewed publications, including 36 international journal papers. Dr Leng is the recipient of the 2018 Institution of Civil Engineers (UK) Baker Medal, 2019 IdEx Post-doctoral Fellowship awarded by Université de Bordeaux (France) and is currently working at WSP as a water resource engineer. She was an invited speaker at 2020 AFMC (Australasian Fluid Mechanics Conference).

Hubert Chanson is Professor of Civil Engineering at the University of Queensland, where he has been since 1990, having previously enjoyed an industrial career for six years. His main field of expertise is environmental fluid mechanics and hydraulic engineering, both in terms of theoretical fundamentals, physical and numerical modelling. He leads a group of 5-10 researchers, largely targeting flows around hydraulic structures, two-phase (gas-liquid and solid-liquid) free-surface flows, turbulence in steady and unsteady open channel flows, using computation, lab-scale experiments, field work and analysis. He has published over 1,250 peer reviewed publications including two dozen of books. He serves on the editorial boards of International Journal of Multiphase Flow, Flow Measurement and Instrumentation, and Environmental Fluid Mechanics, the latter of which he is currently a senior Editor. His Youtube channel is: <https://www.youtube.com/channel/UCm-SedWAjKdQdGWNbCwppqw>.